

# Dynamics of a liquid plug in a capillary tube under cyclic forcing: memory effect and airway reopening

S. Signe Mamba, J. C. Magniez, F. Zoueshtiagh and M. Baudoin<sup>†</sup>

Univ. Lille, CNRS, Centrale Lille, ISEN, Univ. Valenciennes, UMR 8520 - IEMN,  
International laboratory LIA/LICS, F-59000 Lille, France

(Received xx; revised xx; accepted xx)

In this paper, we investigate both experimentally and theoretically the dynamics of a liquid plug driven by a cyclic forcing inside a cylindrical rigid capillary tube. First, it is shown that depending on the type of forcing (flow rate or pressure cycle), the dynamics of the liquid plug can either be stable and periodic, or conversely accelerative and eventually leading to the plug rupture. In the latter case, we identify the source of the instability to be a combination of a flow memory resulting from liquid film deposition on the walls and a lubrication effect, i.e. a reduction of the plug resistance to motion when the walls are prewetted. Second, we show that contrary to unidirectional pressure forcing, cyclic forcing enables breaking of large plugs in confined space though it requires longer times. All the experimentally observed tendencies are quantitatively recovered from an analytical model. This study not only reveals the underlying physics but also opens up the prospect for the simulation of "breathing" of liquid plugs in complex geometries and the determination of optimal cycles for obstructed airways reopening.

**Key words:** Liquid plug, Slug, Bolus, Capillary tube, Cyclic forcing, Airways reopenings

## 1. Introduction

Since the seminal works by [Fairbrother & Stubbs \(1935\)](#), [Taylor \(1961\)](#) and [Bretherton \(1961\)](#), gas-liquid flows in capillary tubes have attracted much interest among different scientific communities due to their widespread occurrence in many natural and engineered fluidic systems such as pulmonary flows ([Grotberg 2011](#)), oil extraction ([Havre \*et al.\* 2000](#); [Di Meglio 2011](#)), flow in porous media ([Lenormand \*et al.\* 1983](#); [Hirasaki \*et al.\* 1985](#); [Dias & Payatakes 1986](#); [Stark & Manga 2000](#)), or microfluidic systems ([Gunther \*et al.\* 2004](#); [Assmann & von Rohr 2011](#); [Ladosz \*et al.\* 2016](#)). In particular, liquid plugs (also called bridges, slugs or boluses) play a fundamental role in pulmonary flows where they can form in healthy subjects ([Burger & Macklem 1968](#); [Hughes \*et al.\* 1970](#)) or in pathological conditions ([Weiss \*et al.\* 1969](#); [Griese \*et al.\* 1997](#); [Wright \*et al.\* 2000](#); [Hohlfeld 2001](#)) due to a capillary or elasto-capillary instability ([Kamm & Schroter 1989](#); [White & Heil 2005](#); [Duclaux & Quéré 2006](#); [Heil \*et al.\* 2008](#); [Grotberg 2011](#); [Dietze & Ruyer-Quil 2015](#)). While obstructed airways reopen naturally during the breathing cycle of healthy subjects, more occluding liquid plugs can dramatically alter the distribution of air in the lungs of patients with pulmonary obstructive diseases, thus leading to severe breathing

<sup>†</sup> Email address for correspondence: michael.baudoin@univ-lille1.fr

difficulties. Conversely, liquid plugs can be used for therapeutic purpose (Van't Veen *et al.* 1998; Nimmo *et al.* 2002): boluses of surfactant are injected inside the lungs of prematurely born infants to compensate for their lack and improve ventilation (Engle & al. 2008; Barber & Blaisdell 2010). A thorough understanding of liquid plugs dynamics is therefore mandatory to improve both treatments of patients suffering from obstructive pulmonary diseases and of prematurely born infants.

When a liquid plug moves inside a cylindrical airway at low capillary number, deformation of the front and rear menisci occurs near the walls and leads to interfacial pressure jumps at the front and rear interfaces. This deformation also leads to the deposition of a liquid film on the walls. From a theoretical point of view, Bretherton (1961) was the first to provide an estimation of the pressure jump and the thickness of the liquid layer at asymptotically low capillary numbers. Bretherton's analysis was later formalized in the framework of matched asymptotic expansions by Park & Homsy (1984) who extended this work to higher order developments. Later on, the dynamics of a meniscus moving on a dry capillary tube was studied both experimentally and theoretically by Hoffman (1975) and Tanner (1979).

These pioneering results were later extended to unfold the effects of wall elasticity (Howell *et al.* 2000), the behavior at larger capillary numbers (Aussillous & Quéré 2000; Klaseboer *et al.* 2014), the effects of surfactants (Waters & Grotberg 2002), the role of a microscopic or macroscopic precursor film (Chebbi 2003), the influence of more complex tube geometries (Wong *et al.* 1995*a,b*; Hazel & Heil 2002), the influence of gravity (Suresh & Grotberg 2005; Zheng *et al.* 2007) or the influence of non-Newtonian properties of the liquid (Guttfinger & Tallmadge 1965; Hewson *et al.* 2009; Jalaal & Balmforth 2016; Laborie *et al.* 2017). These key ingredients have then been combined with conservation laws determining the evolution of plug size and estimation of pressure jump in the bulk of the plug to provide analytical models of the unsteady dynamics of liquid plugs in capillary tubes (Baudoin *et al.* 2013; Magniez *et al.* 2016; Fujioka *et al.* 2016). In particular, Baudoin *et al.* (2013) introduced the long range and short range interactions between plugs to simulate the collective behaviour of a train of liquid plugs. These models were in turn used to determine the critical pressure head required to rupture a liquid plug in a compliant (Howell *et al.* 2000) or rigid prewetted capillary tube (Magniez *et al.* (2016)), or determine the maximum stresses exerted on the walls (Fujioka *et al.* 2016), a fundamental problem for lung injury produced by the presence of liquid plugs in the lung.

It is interesting to note that the dynamics of bubbles (Bretherton 1961; Ratulowski & Chang 1989; Fries *et al.* 2008; Warnier *et al.* 2010) and liquid plugs in capillary tubes look similar from a theoretical point of view, since the interfacial pressure jumps and the deposition of a liquid film on the walls induced by the dynamical deformation of the interfaces can be calculated with the same formula. Nevertheless, there are also fundamental differences, which lead to very different dynamics: Trains of bubble are pushed by a liquid finger whose viscous resistance to the flow is generally higher than the interfacial resistance induced by the presence of the interfaces. In this case, a pressure driven flow is stable and the flow rate remains essentially constant over time. In the case of liquid plugs, the resistance of the plugs to motion is higher than the one of the air in front and behind the plug. This leads to an unstable behavior with an acceleration and rupture of the plugs (Baudoin *et al.* 2013) or a deceleration and the obstruction of the airways (Magniez *et al.* 2016).

From an experimental point of view, Bretherton's interfacial laws have been extensively verified for different systems (bubbles, liquid fingers, foams, ...). Nevertheless, there have been few attempts to compare the unstable dynamics of single or multiple plugs in

capillary tubes to models accounting for the interface and bulk pressure jumps along with mass balance. [Baudoin \*et al.\* \(2013\)](#) showed that their model was able to qualitatively predict the collective accelerative dynamics of multiple plugs in rectangular microfluidic channels. More recently, [Magniez \*et al.\* \(2016\)](#) were able to quantitatively reproduce the acceleration and deceleration of a single liquid plug in a prewetted capillary tube. Their model further provided the critical pressure below which the plug slows down and thickens whereas above it accelerates and ruptures. These experiments were particularly challenging owing to the complexity of controlling the prewetting film thickness and performing the experiments before the occurrence of Rayleigh-Plateau instability. [Huh \*et al.\* \(2007\)](#) measured in realistic experiments the injury caused by the motion of liquid plugs on human airway epithelia deposited at the surface of an engineered microfluidic airway. Later on, [Zheng \*et al.\* \(2009\)](#) quantified the deformation of the walls induced by the propagation of a liquid plug in a flexible microchannel. [Song \*et al.\* \(2011\)](#) employed microfluidic technics to investigate single liquid plug flow in a tree geometry and evidenced the role of the forcing condition on the flow pattern. Finally, [Hu \*et al.\* \(2015\)](#) studied the rupture of a mucus-like liquid plug in a small microfluidic channel.

From a numerical point of view, simulations of liquid plugs in capillary tubes are highly challenging. Indeed, the thin layer of liquid left on the walls requires either adaptive mesh or the use of Boundary Integral Methods to reduce the computational costs. Moreover, the unstable dynamics of the plugs pushed at constant pressure head leads to high variability in the associated characteristic times. [Fujioka & Grotberg \(2004\)](#) were the first to provide numerical simulations of the steady dynamics of a liquid plug in a two-dimensional channel. Later on, they studied the effects of surfactants ([Fujioka & Grotberg 2005](#)), the unsteady propagation ([Fujioka \*et al.\* 2008](#)) in an axisymmetric tube, the effects of gravity ([Zheng \*et al.\* 2007](#)) the role played by the tube's flexibility ([Zheng \*et al.\* 2009](#)) and the motion of Bingham liquid plugs ([Zamankhan \*et al.\* 2012](#)). More recently, [Vaughan & Grotberg \(2016\)](#) studied numerically the splitting of a two dimensional liquid plug at an airway bifurcation.

In all the aforementioned theoretical, experimental and numerical studies, the liquid plugs are pushed either at constant flow rate or at constant pressure head in a single direction. These driving conditions substantially differ from the one in the lung where liquid plug will experience periodic forcing. In this paper, we investigate both experimentally and theoretically the response of liquid plugs to cyclic pressure or flow rate forcing. The experiments are conducted in straight cylindrical glass capillary tubes and compared to an extended theoretical model based on previous developments by [Baudoin \*et al.\* \(2013\)](#) and [Magniez \*et al.\* \(2016\)](#). It is shown that, depending on the type of forcing (flow rate or pressure cycle), the dynamics of the liquid plug can either be periodic with the reproduction of the same cyclic motion over time, or accelerative eventually leading to the plug rupture. In particular, this study discloses the central hysteretic role played by the liquid film deposition on the plug dynamics.

The paper is organized as follows: Section 2 describes the experimental set-up and the mathematical model. Section 3 is dedicated to the comparison of different type of forcings: pressure head and flow rate. In section 4, we compare the efficiency of cyclic and unidirectional forcings for obstructed airways reopening. Finally, concluding remarks and future prospects are provided in section 5.

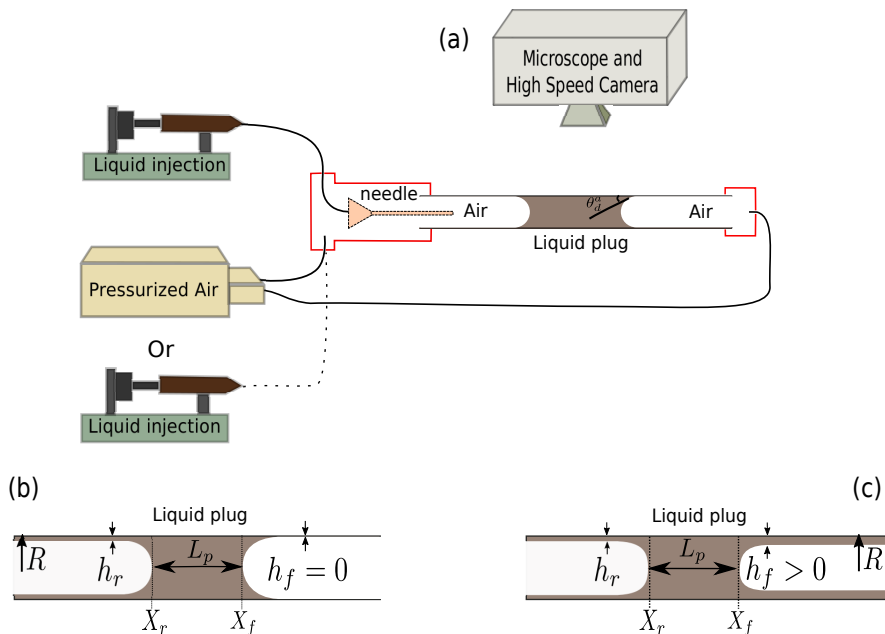


Figure 1. (a) Sketch of the experimental set-up. (b) First half cycle : the liquid plug moves on a dry capillary tube. (c) Following back and forth motions: the liquid plug moves on a prewetted capillary tube.

## 2. Methods

### 2.1. Experimental set-up

The schematic of the experimental set-up is provided in figure 1(a). A perfluorodecalin liquid plug of controlled volume is injected through a needle inside a rigid horizontal cylindrical glass capillary tube (inner radius  $R = 470 \mu\text{m}$ ). Then, air is blown at low flow rate ( $Q = 10 \mu\text{l}/\text{min}$ ) to bring the liquid plug to the center of the channel. Finally, liquid plugs are moved back and forth with either pressure or flow rate cyclic forcings enforced respectively with a MFCS Fluigent pressure controller or a KdScientific 210 programmable syringe pump. For both pressure driven and flow rate driven experiments, the period of oscillation is fixed at  $2T = 4\text{s}$ , with  $T$  the duration of the motion in one direction. It is important to note that during the first half-cycle,  $t \in [0, T]$ , the liquid plug moves along a dry capillary tube (figure 1(b)). The motion of the plug leads to the deposition of a trailing film on the walls of thickness  $h_r$  behind the rear meniscus at position  $X_r(t)$ . Thus, in the subsequent back and forth motion, the front interface of the liquid plug moves on walls prewetted by a layer of thickness  $h_f(X_f)$  (with  $X_f(t) = X_r(t) + L_p(t)$  the position of the front meniscus and  $L_p(t)$  the plug length) as long as it remains on a portion of the channel already visited by the liquid plug (figure 1(c)) in a previous half-cycle.

The glass tubes were cleaned prior to the experiments with acetone, isopropanol, dichloromethane and piranha solutions (a mixture of sulfuric acid ( $\text{H}_2\text{SO}_4$ ) and hydrogen peroxide ( $\text{H}_2\text{O}_2$ )) successively to obtain perfectly wetting surface and prevent dewetting induced by the presence of dust or organic contaminants on the surface. Perfluorodecalin (dynamic viscosity  $\mu = 5.1 \times 10^{-3} \text{Pa}\cdot\text{s}$ , surface tension  $\sigma = 19.3 \times 10^{-3} \text{N}/\text{m}$  and density  $\rho = 1.9 \times 10^{-3} \text{kg}/\text{m}^3$ ) was chosen for its good wetting properties and inertness.

---

parameters	Formula	Maximum value
$\tau_c$	$R/U$	$1.7 \times 10^{-2} \text{ s}$
$\tau_v$	$\rho R^2/\mu$	$8.2 \times 10^{-2} \text{ s}$
$Re$	$\tau_d/\tau_c$	4.9
$Ca$	$\mu U/\sigma$	$7.4 \times 10^{-3}$
$Bo$	$\Delta\rho g R^2/\sigma$	$2.1 \times 10^{-1}$
$We$	$\Delta\rho U^2 R/\sigma$	$3.6 \times 10^{-2}$

---

Table 1. Values of the key parameters associated with the maximal velocity  $U_m$ 

Experiments are recorded using a Photron SA3 high speed camera mounted on a Z16 Leica Microscope at a frame rate of 125 images per second, a trigger time of 1/3000s and a resolution of  $1024 \times 64$  pixels. To prevent image deformation due to the cylindrical shape of the capillary tube, it is immersed in an index-matching liquid. The image analysis is then performed using ImageJ software and Matlab.

## 2.2. Dimensional analysis of the problem

The characteristic parameters in this problem are the radius of the tube  $R$ , the surface tension  $\sigma$ , the liquid density  $\rho$  and viscosity  $\mu$ , and the characteristic speed  $U$  of the liquid plug. From these parameters, one can derive the characteristic convection time  $\tau_c = R/U$ , the characteristic viscous diffusion time  $\tau_v = \rho R^2/\mu$ , the Reynolds number  $Re = \rho U R/\mu$  (comparing inertia to viscous diffusion), the capillary number  $Ca = \mu U/\sigma$  (comparing viscous diffusion to surface tension), the Bond number  $Bo = \Delta\rho g R^2/\sigma$  (comparing gravity effects to surface tension) and finally the Weber number  $We = \Delta\rho U^2 R/\sigma$  (comparing inertia to surface tension). Table 1 summarizes the maximum values of these key dimensionless parameters based on the maximal velocity of the liquid plug  $U_m = 28 \text{ mm/s}$  observed in the present experiments.

Based on the order of magnitude of these dimensionless parameters, a few primary insights can be drawn. The low Bond number and the horizontal position of the tube suggest weak effect of gravity in this problem. The flow in the bulk of the plug remains laminar owing to the moderate values of the Reynolds number. In addition, [Aussillous & Qu  r   \(2000\)](#) studied the impact of inertia on the deposition of a trailing liquid film behind a moving liquid plug. From dimensional analysis and experiments, they introduced a critical capillary number  $Ca_c$  (equal to  $3.6 \times 10^{-1}$  in the present case) above which the effect of inertia becomes significant. In the present experiments, the capillary number is two order of magnitude smaller than this critical value and thus inertia can be neglected in the film deposition process. Finally, [Kreutzer \*et al.\* \(2005\)](#) studied numerically the influence of inertia on pressure drops at liquid/air interfaces. They showed that inertia plays no role for  $Re < 10$  at capillary numbers comparable to the present study. Thus, inertial effects can safely be neglected here. Furthermore, the weak capillary and Weber numbers indicate that surface tension is globally dominant over viscous stresses and inertia. Nevertheless, it is to be emphasized that viscous effects must still be accounted for close to the walls, in the so-called "dynamic meniscus" that is the part of the meniscus deformed by viscous stresses. Finally, since the convection and viscous diffusion times  $\tau_c$  and  $\tau_v$  are two orders of magnitude smaller than the duration of the pressure or flow rate cycles, unsteady term in Navier-Stokes equation can be neglected and the flow can be considered as quasi-static.

### 2.3. Model: pressure driven forcing

In the above context, the liquid plug dynamics can be predicted from a quasi-static pressure balance and a mass balance. We thus adapted a visco-capillary quasi-static model previously introduced by Magniez *et al.* (2016) to include the motion on both dry and prewetted portions of the tube and also the memory effects resulting from a trailing liquid film deposition. Assuming that the pressure losses in the gas phase are negligible compared to that induced by the liquid plug, the total pressure jump  $\Delta P_t$  across a liquid plug can be decomposed into the sum of the pressure jump induced by the presence of the rear interface  $\Delta P_{rear}^{int}$ , the front interface  $\Delta P_{front}^{int}$  and the flow in the bulk of the plug  $\Delta P_{visc}^{bulk}$ :

$$\Delta P_t = \Delta P_{visc}^{bulk} + \Delta P_{rear}^{int} + \Delta P_{front}^{int} \quad (2.1)$$

In the experiments,  $\Delta P_t$  corresponds to the driving pressure head.

Since the flow is laminar, the viscous pressure drop in the bulk of the plug can be estimated from Poiseuille's law:

$$\Delta P_{visc}^{bulk} = \frac{8\mu L_p U}{R^2} \quad (2.2)$$

with  $L_p$ , the plug length, that is to say the distance between the front and rear meniscus  $L_p(t) = X_f(t) - X_r(t)$  as described in figure 1 and  $U = dX_r/dt$  the liquid plug velocity.

The pressure drop across the rear interface of a moving liquid plug at low capillary number is given by Bretherton's formula (Bretherton 1961) :

$$\Delta P_{rear}^{int} = \frac{2\sigma}{R}(1 + 1.79(3Ca)^{2/3}) \quad (2.3)$$

Finally, the Laplace pressure drop across the front meniscus depends on the apparent dynamic contact angle  $\theta_d^a$  according to the formula (in the limit of low capillary number and thus  $\theta_d^a$ ):

$$\Delta P_{front}^{int} = -\frac{2\sigma \cos \theta_d^a}{R} \approx -\frac{2\sigma(1 - \theta_d^{a2}/2)}{R} \quad (2.4)$$

Choosing the Laplace pressure jump  $2\sigma/R$  as the characteristic pressure scale, and the tube radius  $R$  as the characteristic length scale, the dimensionless pressure jump across the liquid plug becomes:

$$\Delta \tilde{P}_t = 4\tilde{L}_p Ca + 1.79(3Ca)^{2/3} + \frac{\theta_d^{a2}}{2} \quad (2.5)$$

The index  $\sim$  indicates dimensionless functions.

In order to achieve a closed set of equation, two additional equations must be derived. They are (i) the relation between the apparent dynamic contact angle of the front meniscus  $\theta_d^a$  and the capillary number  $Ca$  and (ii) an equation determining the evolution of the plug length  $\tilde{L}_p$ . The first relation depends on the wetting state of the tube walls ahead of the liquid plug:

When the liquid plug moves on a *dry substrate*, this relation is given by Hoffman-Tanner's law valid at low capillary numbers:

$$\theta_d^a = E Ca^{1/3} \quad (2.6)$$

with  $E$  a numerical constant of the order of 4 – 5 for a dry cylindrical capillary tube as reported by Hoffman (1975) and Tanner (1979). For a liquid plug moving on a *prewetted substrate*,  $\theta_d^a$  can be calculated from Chebbi's law (Chebbi 2003), which can be simplified

at low capillary number through a second order Taylor expansion (Magniez *et al.* 2016):

$$\theta_a^a = \frac{-1 + \sqrt{1 + 4CD}}{2C} \quad (2.7)$$

with:

$$A = (3Ca)^{-2/3} \tilde{h}_f \quad (2.8)$$

$$B = (3Ca)^{1/3} \quad (2.9)$$

$$C = \frac{1}{\log(10)} \left( \frac{b_1}{2} + b_2 \log_{10}(A) + \frac{3b_3}{2} [\log_{10} A]^2 \right) B \quad (2.10)$$

$$D = \left( b_0 + b_1 \log_{10}(A) + b_2 [\log_{10}(A)]^2 + b_3 [\log_{10}(A)]^3 \right) B \quad (2.11)$$

$$b_0 \approx 1.4, \quad b_1 \approx -0.59, \quad b_2 \approx -3.2 \times 10^{-2}, \quad \text{and} \quad b_3 \approx 3.1 \times 10^{-3} \quad (2.12)$$

Since  $CD \ll 1$  at low capillary number (in the present experiments  $CD < 5 \times 10^{-2}$ ), this equation can further be simplified into:

$$\theta_a^d = D = FCa^{1/3}$$

with  $F = 3^{1/3} \left( b_0 + b_1 \log_{10}(A) + b_2 [\log_{10}(A)]^2 + b_3 [\log_{10}(A)]^3 \right)$ .

The next step is to determine the dimensionless plug length  $\tilde{L}_p$ . A simple mass balance between the fluid collected from the fluid layer lying ahead the plug (of thickness  $h_f$ ) and the trailing liquid film (of thickness  $h_r$ ) deposited behind the plug gives:

$$dV = (\pi R^2 - \pi(R - h_f)^2) dX_f - (\pi R^2 - \pi(R - h_r)^2) dX_r \quad (2.13)$$

with  $V = \pi R^2 L_p$  the volume of the plug. Finally, with  $dX_r = U dt$  and  $dX_f = \frac{(R - h_r)^2}{(R - h_f)^2} dX_r$ , we obtain:

$$\frac{dL_p}{dt} = \left[ \frac{(R - h_r)^2}{(R - h_f)^2} - 1 \right] U \quad (2.14)$$

Using the capillary time scale,  $\mu R / \sigma$ , as the characteristic time scale, this equation can be rewritten in the dimensionless form:

$$\frac{d\tilde{L}_p}{d\tilde{t}} = \left[ \frac{(1 - \tilde{h}_r)^2}{(1 - \tilde{h}_f)^2} - 1 \right] Ca \quad (2.15)$$

The last essential point is to determine the thicknesses of the liquid film lying in front and left behind the liquid plug  $h_r$  and  $h_f$  respectively. The thickness of the trailing film can be calculated from an extension of Bretherton's law introduced by Aussillous & Qu  r   (2000). This thickness only depends on the velocity of the plug  $U$ , that is to say in dimensionless form only on the capillary number  $Ca$ :

$$\tilde{h}_r = \frac{1.34Ca^{2/3}}{1 + 2.5 \times 1.34Ca^{2/3}} \quad (2.16)$$

Finally, the thickness  $\tilde{h}_f$  depends on the history of the plug motion. Indeed, the capillary tube is initially dry. Thus, for a cyclic motion, the liquid film lying ahead of the plug at position  $X_f^N$  during the half-cycle  $N$  comes from the deposition of a trailing film behind the plug at the same position  $X_r^{N-1} = X_f^N$  during the half cycle  $N - 1$ . In order to



determine  $\tilde{h}_f$ , the thickness of the liquid film deposited on the walls must therefore be kept in memory and then taken as an entry when the plug moves back to the same location. If the plug moves to a location never visited before, then the tube is dry,  $\tilde{h}_f = 0$  and the pressure jump for the front interface corresponds to the dry version. This analysis shows that the liquid film acts as a memory of the liquid plug motion, that is nevertheless erased at each back and forth motion.

To summarize, the complete nonlinear system of equations that need to be solved to determine the evolution of the plug is:

$$\Delta\tilde{P}_t = \begin{cases} 4\tilde{L}_p Ca + \left(3.72 + \frac{E^2}{2}\right) Ca^{2/3}, & \text{if dry} \\ 4\tilde{L}_p Ca + \left(3.72 + \frac{F^2}{2}\right) Ca^{2/3}, & \text{if prewetted} \end{cases} \quad (2.17)$$

$$F = 3^{1/3} \left( b_0 + b_1 \log_{10}(A) + b_2 [\log_{10}(A)]^2 + b_3 [\log_{10}(A)]^3 \right) \quad (2.18)$$

$$A = (3Ca)^{-2/3} \tilde{h}_f \quad (2.19)$$

$$\frac{d\tilde{X}_r}{d\tilde{t}} = Ca, \quad \tilde{X}_f = \tilde{X}_r + \tilde{L}_p \quad (2.20)$$

$$\frac{d\tilde{L}_p}{d\tilde{t}} = \left[ \frac{(1 - \tilde{h}_r)^2}{(1 - \tilde{h}_f)^2} - 1 \right] Ca \quad (2.21)$$

$$\tilde{h}_r = \frac{1.34Ca^{2/3}}{1 + 2.5 \times 1.34Ca^{2/3}} \quad (2.22)$$

$$\tilde{h}_f(\tilde{X}_f) \text{ is obtained from the memory of the liquid film deposition} \quad (2.23)$$

At each change of flow direction, the front meniscus becomes the rear meniscus and vice versa. The pressure balance in the dry and prewetted tubes share a relatively similar expression, but the coefficient  $E$  remains constant while  $F$  depends both on  $Ca$  and  $\tilde{h}_r$ . This system of equations is solved numerically with an Euler method. Since the dynamics is accelerative, an adaptive time step refinement is used. It consists in keeping the spatial displacement over a time step constant:  $\Delta\tilde{t} = \Delta\tilde{x}/Ca$  with  $\Delta\tilde{x}$  constant. Convergence analysis on  $\Delta\tilde{x}$  was performed for the calculations presented in this paper.

#### 2.4. Validation of the model for unidirectional pressure forcing in a dry capillary tube

Magniez *et al.* (2016) validated the constitutive laws summarized in the previous section through careful comparison with experiments of the motion of liquid plugs in *prewetted* capillary tubes driven by a constant pressure head. This section is dedicated to the validation of the constitutive laws for the motion of liquid plugs in *dry* capillary tubes driven by an unidirectional pressure driving (represented on figure 2) and in particular the determination of the Hoffman-Tanner constant  $E$  (an essential parameter in the analytical model).

In such configuration (figure 3), the deposition of a trailing film behind the plug leads to the reduction of the plug length (figure 3(b)) and eventually its rupture when the front and rear interface meet (see figure 3(a) at time  $t = 3s$ ). This process is unsteady and highly accelerative as seen on figure 3(c). From  $t = 0$  to  $t = 2s$  this acceleration is mostly related to the increase in the pressure head (see figure 2). After  $t = 2s$ , the acceleration goes on and is even exacerbated close to the plug rupture, while the pressure head reaches a plateau. This behaviour can be understood by rewriting equation 2.17 under a form reminiscent of Ohm's law:  $\Delta\tilde{P}_t = \tilde{R}_t Ca$ , with  $\tilde{R}_t = (\tilde{R}_v + \tilde{R}_i^r + \tilde{R}_i^f)$  the dimensionless



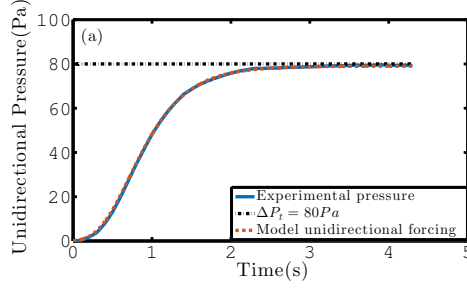


Figure 2. Unidirectional pressure forcing imposed by the pressure controller. Blue solid line: pressure magnitude measured with an integrated pressure sensor. Red dashed line: approximation of the pressure driving by the so-called Gompertz function  $\Delta P_t = 78e^{-6e^{-3t}}$  used in the simulations as the driving pressure head since it fits well with the experimental signal. Black dashed-dotted line: asymptote  $\Delta P_t = 80$  Pa when  $t \rightarrow \infty$ .

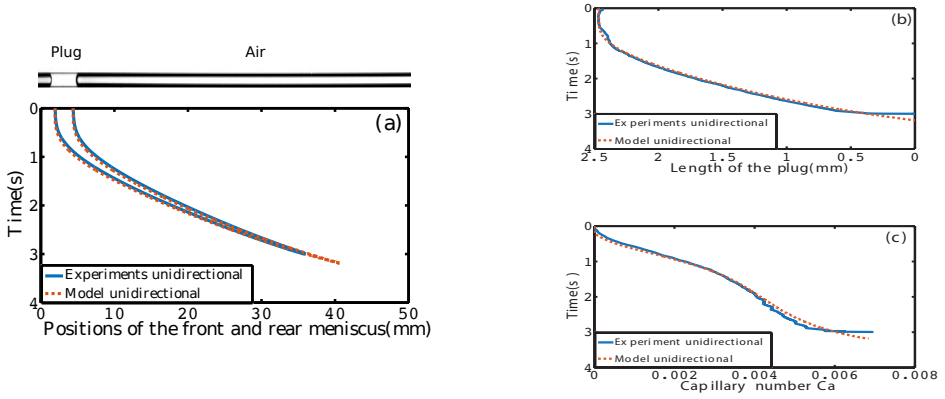


Figure 3. Temporal evolution of a liquid plug of initial length  $L_0 = 2.5\text{mm}$  pushed with a unidirectional driving pressure (represented on figure 2) in a dry capillary tube. (a) Position of the rear and front meniscus. (b) Evolution of the plug length. (c) Evolution of the plug dimensionless speed, i.e. the capillary number  $Ca$ . Blue curves correspond to experiments and the red dashed curves are obtained from simulations of equations 2.17 to 2.23.

global resistance to the flow,  $\tilde{R}_v = 4\tilde{L}_p$ ,  $\tilde{R}_i^f = E^2/2 Ca^{-1/3}$  and  $\tilde{R}_i^r = 3.72 Ca^{-1/3}$  the viscous, front and rear interface resistances respectively. From this form of the pressure balance, we see that the reduction of the plug length  $\tilde{L}_p$  leads to a reduction of the viscous resistance  $\tilde{R}_v$  and thus, at constant pressure driving  $\Delta\tilde{P}_t$ , to an increase of the capillary number. This increase in the capillary number is strengthened by a decrease of the interfacial resistance  $\tilde{R}_i = \tilde{R}_i^f + \tilde{R}_i^r$ , since  $R_i$  is proportional to  $Ca^{-1/3}$ . Finally, the increase of the trailing film thickness with the capillary number (equation 2.22) implies that the whole process (fluid deposition and plug motion) accelerate progressively as can be seen on figure 3.

Many experiments have been performed for different initial plug lengths and compared with the numerical solutions of equations 2.17 to 2.23 (dry version with  $\tilde{h}_f = 0$ ). In the simulations, a Gompertz function  $\Delta P_t = 78e^{-6e^{-3t}}$  was used as the driving pressure head due to its excellent match with the pressure head measured experimentally at the exit

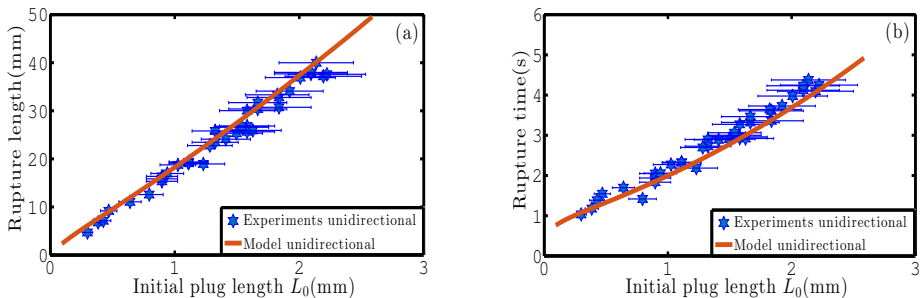


Figure 4. Evolution of (a) the rupture length and (b) the rupture time of a liquid plug pushed with a unidirectional pressure head of the form  $\Delta P_t = 59e^{-6e^{-3.5t}}$  in a dry capillary tube as a function of the initial plug length  $L_0$ . The blue stars represent experiments and the red curves simulations.

of the the pressure controller with an integrated pressure sensor (see figure 2, blue line corresponds to experimental signal and red line to best fit with Gompertz function). The complex shape of the pressure head is the result of the pressure controller response time (the command is a constant pressure  $P_o = 80 Pa$  starting at  $t = 0$ ). The only adjustable parameter in the model is the Hoffman-Tanner constant  $E$  appearing in equation 2.17. The best fit between experiments and theory was achieved for  $E = 4.4$ , a value close to the coefficient 4.3 obtained by Bico & Qu  r   (2001) in their experiments on falling of liquid slugs in vertical dry capillary tubes. With this value, an excellent prediction of the plug dynamics is achieved for all experiments (see e.g. figure 3 where blue solid lines correspond to experiments and red dashed lines to simulations). In particular, this model enables a quantitative prediction of the rupture length, defined as the portion of the tube  $L_d = \max(X_f) - \min(X_r)$  visited by the liquid plug before its rupture (figure 4(a)), and the rupture time, which is the total time elapsed between the beginning of the experiment and the plug rupture (figure 4(b)).

### 3. Cyclic forcing of liquid plugs

This section is dedicated to the dynamics of liquid plugs under cyclic forcing. In the first subsection, the influence of the forcing configuration (pressure or flow rate) is examined. The second subsection enlightens the fundamental role played by hysteretic effects resulting from fluid deposition on the walls.

#### 3.1. Influence of the driving condition: pressure head versus flow rate

In this first subsection, the responses of liquid plugs to two types of forcings are compared: (i) a cyclic flow rate imposed by a syringe pump (represented on figure 5(a), blue line) and (ii) a pressure cycle imposed by a pressure controller (represented on figure 5(b), blue line). This latter forcing has a complex temporal shape owing to the response time of the pressure controller. It is well approximated by the following combination of Gompertz functions (see figure 5(b), red dashed line):

$$\begin{cases} \Delta P_t = 78e^{-6e^{-3t}} & \text{for } t \in [0, T] \\ \Delta P_t = (-1)^n (P_c - P_d) & \text{for } t \in [n, (n+1)T] \\ P_c = 78e^{-3e^{-3(t-nT)}} \\ P_d = 78e^{-1.4(t-nT)} e^{-0.02 * e^{-1.4 * (t-nT)}} \end{cases} \quad (3.1)$$

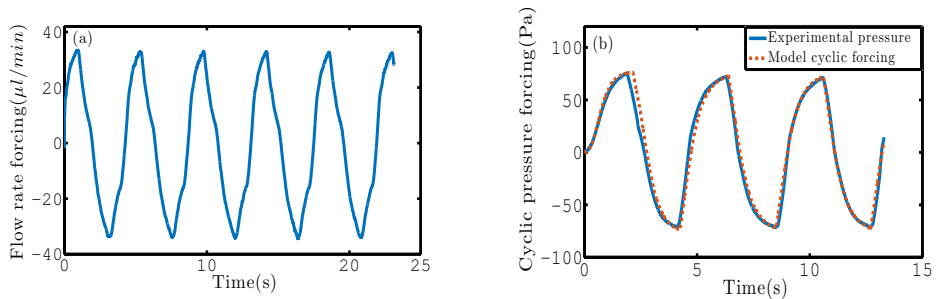


Figure 5. (a) Flow rate and (b) pressure cyclic forcing imposed experimentally with respectively a syringe pump and a pressure controller. Blue solid line: experimental values measured with sensors. Red dashed line: fit of the pressure cyclic forcing measured experimentally with the analytical expression:  $\Delta P_t = 78e^{-6e^{-3t}}$  for  $t \in [0, T]$ ,  $\Delta P_t = (-1)^n(P_c - P_d)$  for  $t \in [nT, (n+1)T]$  with  $P_c = 78e^{-3e^{-3(t-nT)}}$  and  $P_d = 78e^{-1.4(t-nT)}e^{-0.02e^{-1.4*(t-nT)}}$ ,  $T = 2.15$  s the half period and  $n \in \mathbb{N}^*$ .

with  $T = 2.15$  s the half period and  $n \in \mathbb{N}^*$  for cyclic forcing.

Two extremely different behaviors are evidenced in these two cases: For a cyclic *flow rate* forcing (figure 6(a),(b),(c) and movie S1), the liquid plug dynamics is periodic and stable (see phase portrait on figure 7(a)). Indeed, the plug velocity and positions are directly imposed by the motion of the syringe pump, thus:  $U(t+2T) = U(t)$  (figure 6(b)) and  $X_r(t+2T) = X_r(t)$  (figure 6(a)). Moreover, since (i) the film deposition process solely depends on the plug velocity and (ii) the fluid recovery at half cycle  $N$  depends on the fluid deposition at half cycle  $N-1$ , the mass balance is null over each cycle and the evolution of the plug size is also periodic:  $L_p(t+2T) = L_p(t)$  (figure 6(c)). It is interesting to note that the initial wall wetting condition plays little role in this process; it only affects the mass balance during the first half cycle and thus determines the plug size  $L_p((2n+1)T)$  with  $n \in \mathbb{N}$ . This wetting condition is indeed erased by the backward motion during the second half cycle and the plug evolution is then only dictated by the temporal shape of the flow rate cycle.

The liquid plug undergoes a very different evolution for a periodic *pressure* forcing (figure 6(d),(e),(f) and movie S2). In this case, the plug velocity and position are no more enforced by the driving condition and depend only on the evolution of the resistance of the plug to motion. For the forcing condition represented on figure 5(b), it is observed that (i) the plug travels on a longer portion of the tube at each cycle (figure 6(d)), (ii) the dimensionless velocity of the plug (the capillary number) is no more cyclic but increases progressively at each cycle,  $U(t+2T) > U(t)$  (figure 6(e)) and (iii) the size of the plug diminishes ( $L_p(t+2T) < L_p(t)$ ), eventually leading to its rupture (figure 6(f)). These phenomena are of course related since a larger plug velocity leads to more liquid deposition and thus a diminution of the plug size. Conversely, the cyclic diminution of the plug size leads to a decrease in the viscous resistance (the same process as described in subsection 2.4). Nevertheless this mechanism does not explain the origin of this hysteretic accelerating behaviour clearly evidenced in the phase portrait (figure 7(b)).

### 3.2. Memory effects and hysteretic behaviour

Such a hysteretic behaviour requires a flow memory. In the absence of memory, the plug would be driven by the same boundary conditions at each cycle, necessarily resulting in a periodic motion since the evolution is quasi-static. With the present model, we were able

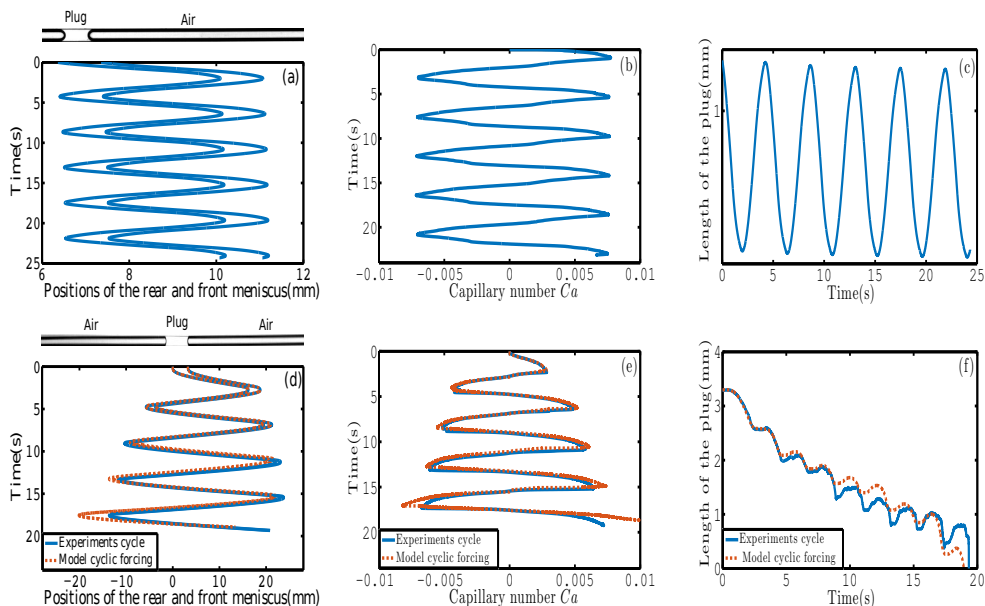


Figure 6. (a), (b), (c) Temporal evolution of a single liquid plug of initial length  $L_0 = 1.05$  mm pushed with the cyclic flow rate forcing represented on figure 5(a), see also movie S1. (a) Positions of the menisci. (b) Evolution of the dimensionless velocity of the rear meniscus (capillary number). (c) Evolution of the plug length. (d), (e), (f) Temporal evolution of a single liquid plug of initial length  $L_0 = 3.3$  mm pushed with the pressure cyclic forcing represented on figure 5(b), see also movie S2. (d) Position of the front and rear menisci. (e) Evolution of the dimensionless velocity of the rear meniscus (capillary number). (f) Evolution of the plug length. In all these figures blue lines represent experiments and red dashed lines simulations obtained from equations 2.17 to 2.23.

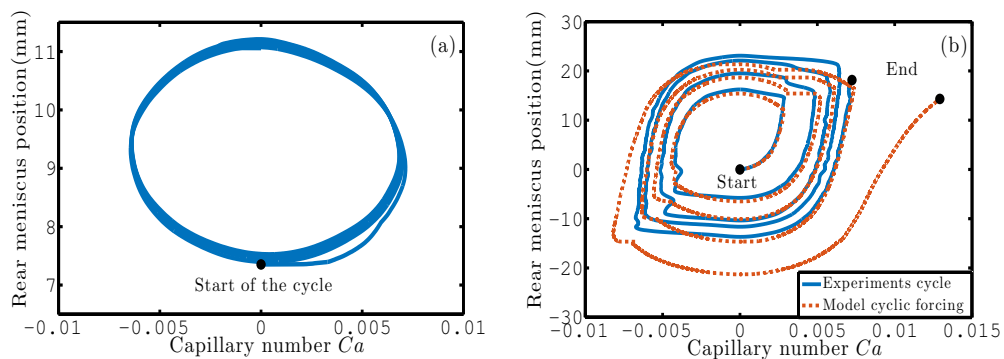


Figure 7. Phase portrait showing the evolution of the position of the rear meniscus as a function of the capillary number  $Ca$ . (a) Cyclic flow rate forcing and (b) cyclic pressure forcing. The blue curves correspond to experiments and the red dashed line to simulations.

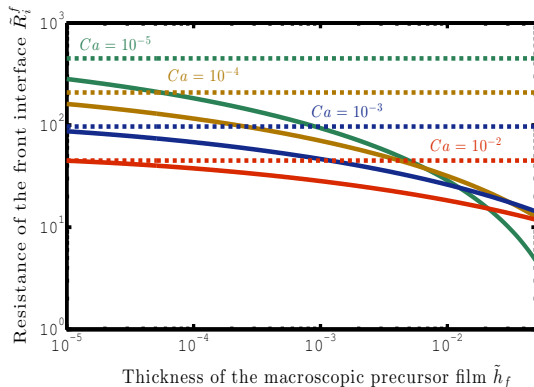


Figure 8. Solid lines: dimensionless front interface resistance  $\tilde{R}_i^f$  at different capillary numbers  $Ca$  as a function of the prewetting film thickness  $\tilde{h}_f$ . Dashed lines: dimensionless front interface resistance for dry capillary tubes. These curves show (i) that the interfacial resistance is systematically lower for prewetted capillary tubes than for dry capillary tubes and (ii) that for prewetted capillary tubes, the interfacial resistance decreases with the thickness of the prewetting film  $\tilde{h}_f$

to accurately reproduce the liquid plug dynamics (figure 6(d),(e),(f), red dashed line) and we analyzed the origin of this memory effect. The analysis shows that the hysteresis originates from a combination of the liquid film deposition and a "lubrication effect", i.e. the reduction of the front interface resistance  $\tilde{R}_i^f = (F^2/2)Ca^{-1/3}$  as the thickness of the prewetting film  $\tilde{h}_f$  is increased (see equation 2.19 and figure 8). Indeed, at each back and forth motion, the liquid plug leaves on the walls a film layer whose thickness keeps a memory of the plug velocity during the corresponding half-cycle (since  $\tilde{h}_f$  depends on  $Ca$ ). The scenario is thus the following: During the first half cycle, the liquid plug moves on a dry capillary tube and leaves a liquid film behind it on the walls. This liquid film lubricates the passage of the plug during the back motion, leading to a drastic reduction of the front interface resistance (figure 8) and thus, a higher plug speed. Then the same mechanism is reproduced during the following cycles: Since the speed is increased at each cycle, the plug leaves more liquid on the walls, leading again to a reduction of the interfacial resistance through a lubrication effect. To demonstrate that the lubrication effect is indeed responsible for the deviation from a periodic dynamics, we simulated the plug behaviour when the front interface resistance  $\tilde{R}_i^f$  is kept constant (figure 9(b)). The simulations show that, in this case, the plug undergoes a quasi-periodic motion.

This analysis shows the central role played by the initial wetting condition. The successive accelerations at each half-cycle all originate from the transition between a dry and a prewetted capillary tube during the first cycle, which led to a massive acceleration of the plug in the back motion. In theory, the opposite behavior (plug cyclic slow down and growth) might be observed in a prewetted capillary tube depending on the thickness of the prewetting film and the amplitude of the pressure driving as was already observed by Magniez *et al.* (2016) for unidirectional constant pressure forcing.

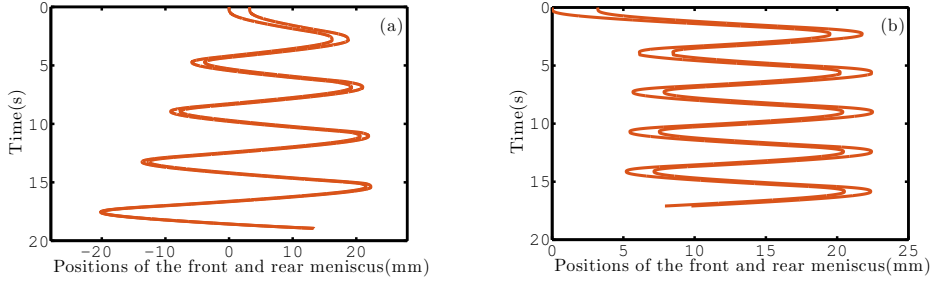


Figure 9. Simulations with equations 2.17 to 2.23 of the positions of the front and rear menisci of a liquid plug of initial size  $L_0 = 1.05$  mm pushed with the cyclic pressure driving represented on figure 5(b). (a) The model takes into account the evolution of the front interface resistance  $\tilde{R}_i^f$  as a function of the thickness of the prewetting film  $\tilde{h}_r$  (equations 2.18 and 2.19). (b) The front interface resistance is kept constant ( $F = E$ ).

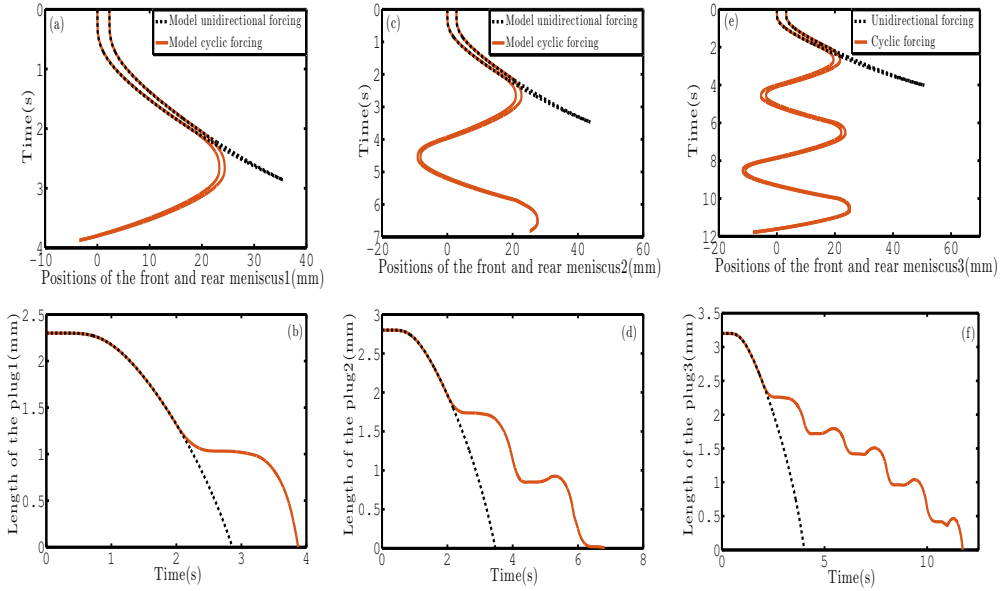


Figure 10. Spatiotemporal evolution of plugs of initial lengths  $L_1 = 2.2$  mm (a,b),  $L_2 = 2.8$  mm (c,d) and  $L_3 = 3.2$  mm (e,f) pushed either with a unidirectional pressure driving (black dotted line) or with a cyclic pressure driving (red dotted line). (a), (c), (e): Position of the rear and front menisci. (b), (d), (f): Evolution of the plug size.

#### 4. Cyclic motion vs direct rupture of the plug under pressure forcing

In this last section, we compare experimentally and theoretically the time and space required to break a liquid plug with either a unidirectional or a cyclic pressure forcing with the same magnitude. The two driving conditions used for this comparison are represented respectively on figure 2 and figure 5(b). As previously mentioned, their temporal evolution can be approximated respectively by the Gompertz function  $\Delta P_t = 78e^{-6e^{-3t}}$  and the equations 3.1.

Figure 10 compares theoretically the dynamics of liquid plugs of increasing sizes for

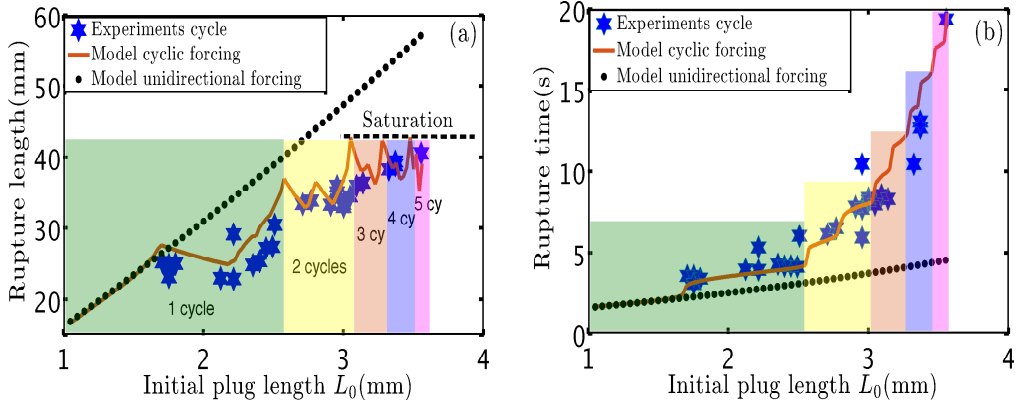


Figure 11. (a) Rupture length and (b) rupture time of a liquid plug pushed with a cyclic pressure driving given by equation 3.1 as a function of their initial lengths  $L_0$ . Blue stars correspond to experiments and the red solid curve to simulations. The black dots show the simulated trend for a unidirectional pressure driving.

unidirectional and cyclic pressure driving. This figure shows (i) that plug rupture and thus airways reopening is obtained in a longer time but in a more confined space with a cyclic forcing compared to a unidirectional pressure forcing and (ii) that the difference between these two driving conditions increases with the number of cycles and hence with the initial size of the liquid plug. This tendency has been verified experimentally and theoretically on a large number of initial plug lengths. The results are summarized in figure 11. Figures 11(a) and (b) show respectively the rupture length (the portion of the tube visited by the liquid plug before its rupture) and the rupture time (the time required for the plug to rupture) as a function of the plug initial length,  $L_0$ . In these two figures, the blue stars and the solid red line correspond respectively to experiments and simulations for a *cyclic* pressure driving, while the black dots corresponds to simulations with a *unidirectional* pressure driving. The successive cycles are highlighted with different colors. This figure shows again excellent agreement between experimental data and numerical predictions for up to 5 cycles (figure 11), underlining that the model summarized in equations 2.17 to 2.23 captures the main physics.

As long as the liquid plug breaks during the first half cycle, the cyclic forcing (red solid line) and the unidirectional forcing (black dotted line) are of course equivalent. When the plug starts going back (for initial length  $L_0 \approx 1.7$  mm) brutal changes in the tendencies are observed: the rupture length starts decreasing (figure 11(a)), while the increase in the rupture time is on the contrary exacerbated (figure 11(b)). For larger plug lengths, the number of cycles required to achieve plug rupture increases rapidly. Since each change in the plug flow direction is associated with some sharp fluctuations of the rupture length, this increase in the number of cycles leads to a saturation of the rupture length (figure 11(a)). This is very different from the relatively linear trend predicted by our simulations (black dots) and observed experimentally on figure 4 for a unidirectional forcing. This saturation means that there is a maximal distance that a liquid plug can travel regardless of its size for a prescribed pressure cycle. Therefore, the plug rupture induced by a periodic forcing is a spatially bounded phenomenon. An interesting point is that, despite this confinement, the plug rupture remains possible due to the hysteretic effects that enable a progressive acceleration of the liquid plug at each cycle, even if the liquid plug moves on the same portion of the tube.



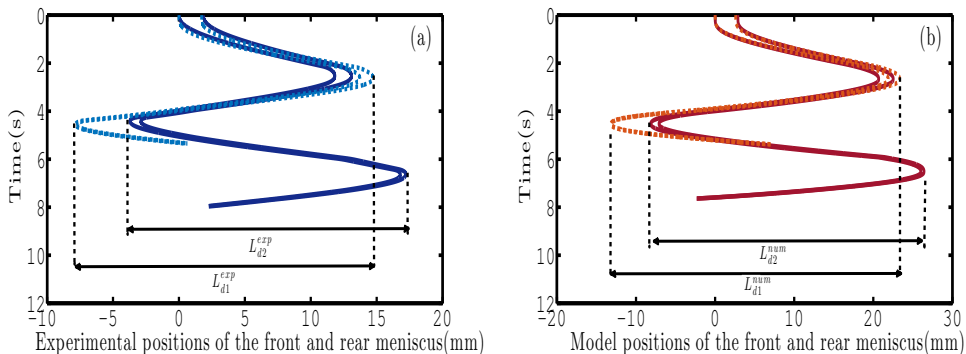


Figure 12. (a) Experimental investigation and (b) numerical investigation of the rupture length of two liquid plugs of close initial lengths. The initial length of the plug in dashed lines  $L_1 = 2.5$  mm is smaller than the initial length of the plug in solid line  $L_2 = 2.85$  mm but nevertheless travels on a larger distance  $L_{d1} > L_{d2}$  before its rupture. The evolution of these two plugs can also be seen on supplementary movies S3 and S4 respectively.

To understand the decrease in the rupture length observed when the flow direction is changed, we plotted the experimentally observed (figure 12(a)) and numerically predicted (figure 12(b)) spatiotemporal diagrams of the evolution of two plugs with initial lengths  $L_1 = 2.5$  mm (movie S3) and  $L_2 = 2.85$  mm (movie S4) in a region where the rupture length is decreasing when the initial plug length is increased. The experiments were performed with a different pressure driving magnitude  $P_o = 60$  Pa than for figure 11. So the positions of these two points in the rupture length graph are represented on figure 13 in Appendix A (encircled points). In figure 12 the dashed lines corresponds to  $L_1 = 2.5$  mm and the solid lines to  $L_2 = 2.85$  mm. The experimental (figure 12(a), blue line) and numerical trends (figure 12(b), red line) are similar. These figures show that the largest plug requires less space to break than the smallest plug  $L_{d1} > L_{d2}$ . The origin of this rather counterintuitive behaviour again lies in memory effects. Since these two plugs are pushed with the same pressure head, the smallest plug with the lowest bulk resistance moves faster, leaves more liquid on the walls than the bigger one and thus goes further during the first half-cycle. When the sign of the pressure head is inverted, the smallest liquid plug will move on a more prewetted channel and thus (i) it will travel faster (since lubrication effects reduce its resistance to motion) and (ii) it will recover more liquid, thus slowing down the plug size decrease through the mass balance. The combination of these two effects enables the plug to reach a deeper location in the tube.

On the other hand, the comparison between unidirectional and cyclic forcing indicates that more time is required to break liquid plugs for cyclic motion than straight motion (figure 11(b)). This is simply the result of the mass balance. As the liquid plug moves back and forth on prewetted capillary tubes, it recovers some liquid while it doesn't when it moves only on a dry capillary tube. This slows down the plug size evolution. It is important to note that for unidirectional driving, we only considered dry tubes. This last result would of course be mitigated in prewetted capillary tubes.

As a conclusion of this section, large liquid plug breaking is achieved in a more confined space but in longer time with a cyclic forcing than with a unidirectional pressure forcing.

## **5. Conclusion**

Despite its occurrence in practical situations such as pulmonary flows in pathological conditions, the specificity of the response of liquid plugs to cyclic driving has not been studied so far experimentally and theoretically. The present results show that the dynamics and rupture of a liquid plug strongly depends on the type of forcing. A flow rate cyclic forcing results in periodic oscillations of the plug and no rupture. On the contrary, a pressure cyclic forcing enables airway reopening through a progressive acceleration of the liquid plug dynamics and reduction of its size. This departure from a periodic response originates from the coupling between a memory effect played by the liquid film deposition process and a lubrication effect. In addition, this study shows that the rupture of a liquid plug with a prescribed pressure cycle is a spatially bounded phenomenon regardless of the initial plug length. In other words, large plug can be ruptured in a limited space with a cyclic forcing, while more and more space is required to break plugs of increasing size with a unidirectional forcing. The trade-off is that more time is nevertheless required to reopen airways with a cyclic forcing.

The analysis of the underlying physics was achieved through a comparison of extensive experimental data to a reduced dimension model. This model quantitatively predicts the plug behaviour for the numerous pressure cycles studied in this paper. Moreover it is in principle valid for any pressure cycle in its range of validity: low capillary, Reynolds and Bond numbers. Combined with constitutive laws for the plug divisions at bifurcation, it might serve as a basis to simulate cyclic plug dynamics in more complex geometries, or even the dynamics of mucus plugs in distal pulmonary airways. In this case however, complementary elements such as the influence of walls elasticity, the non-Newtonian fluid properties of mucus or the presence of pulmonary surfactant should be implemented to achieve realistic simulations. Such models would open tremendous perspectives, such as the "virtual testing" of new strategies to improve airways clearance for patients suffering from chronic obstructive pulmonary disease or cystic fibrosis.

## **Acknowledgements**

The author acknowledge the financial support from Université de Lille.

## **Appendix A. Supplementary figure.**

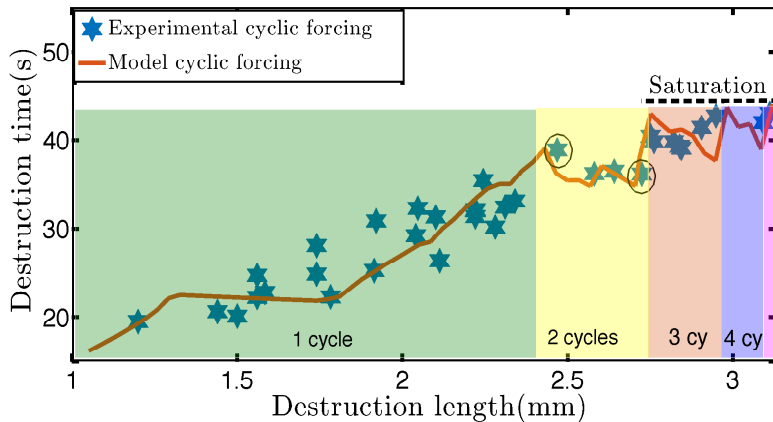


Figure 13. Rupture length of a liquid plug pushed with a cyclic pressure driving given by the analytical function  $\Delta P_t = 59e^{-6e^{-3.5t}}$  for  $t \in [0, T]$ ,  $\Delta P_t = (-1)^n(P_c - P_d)$  for  $t \in [nT, (n+1)T]$  with  $P_c = 59e^{-2.2e^{-3.5(t-nT)}}$  and  $P_d = 59e^{-1.1(t-nT)}e^{-0.06e^{-1.1*(t-nT)}}$ ,  $T = 2.1$  s the half period and  $n \in \mathbb{N}^*$ . Blue stars correspond to experiments, the red curve is the result from our simulations. The encircled experimental points correspond to plugs of initial lengths  $L_1 = 2.5$  mm and  $L_2 = 2.85$  mm, whose evolutions are compared in figure 12.

## REFERENCES

- ASSMANN, N. & VON ROHR, P. R. 2011 Extraction in microreactors: intensification by adding an inert gas phase. *Chem. Eng. Process* **50** (8), 822–827.
- AUSSILLOUS, P. & QUÉRÉ, D. 2000 Quick deposition of a fluid on the wall of a tube. *Phys. Fluids* **12** (10), 2367–2371.
- BARBER, M. & BLAISDELL, C. J. 2010 Respiratory causes of infant mortality: progress and challenges. *Am. J. Perinat.* **27** (07), 549–558.
- BAUDOIN, M., SONG, Y., MANNEVILLE, P. & BAROUD, C. N. 2013 Airway reopening through catastrophic events in a hierarchical network. *Proc. Natl. Acad. Sci. U. S. A.* **110** (3), 859–864.
- BICO, J. & QUÉRÉ, D. 2001 Falling slugs. *J. Colloid Interf. Sci.* **243** (1), 262–264.
- BRETHERTON 1961 The motion of long bubbles in tubes. *J. Fluid Mech.* **10** (02), 166–188.
- BURGER, E. J. & MACKLEM, P. 1968 Airway closure: demonstration by breathing 100 percent  $O_2$  at low lung volumes and by  $N_2$  washout. *J. Appl. Physiol.* **25** (2), 139–148.
- CHEBBI, R. 2003 Deformation of advancing gas-liquid interfaces in capillary tubes. *J. Colloid Interf. Sci.* **265** (1), 166–173.
- DI MEGLIO, F. 2011 Dynamics and control of slugging in oil production. PhD thesis, Ecole Nationale supérieure des mines de Paris.
- DIAS, M. M. & PAYATAKES, A. C. 1986 Network models for two-phase flow in porous media part 1. immiscible microdisplacement of non-wetting fluids. *J. Fluid Mech.* **164**, 305–336.
- DIETZE, G. F. & RUYER-QUIL, C. 2015 Films in narrow tubes. *J. Fluid Mech.* **762**, 68–109.
- DUCLAUX, V., CLANET C. & QUÉRÉ, D. 2006 The effects of gravity on the capillary instability in tubes. *J. Fluid Mech.* **556**, 217–226.
- ENGLE, W. A. & AL. 2008 Surfactant-replacement therapy for respiratory distress in the preterm and term neonate. *Pediatrics* **121** (2), 419–432.
- FAIRBROTHER, F. & STUBBS, A. E. 1935 Studies in electro-endosmosis. *J. Chem. Soc.* pp. 527–529.
- FRIES, D. M., TRACHSEL, F. & VON ROHR, P. R. 2008 Segmented gas-liquid flow characterization in rectangular microchannels. *Int. J. Multiphas. Flow* **34** (12), 1108–1118.

- FUJIOKA, H. & GROTBORG, J. B. 2004 Steady propagation of a liquid plug in a two-dimensional channel. *J. Biomed. Eng.* **126** (5), 567–577.
- FUJIOKA, H. & GROTBORG, J. B. 2005 The steady propagation of a surfactant-laden liquid plug in a two-dimensional channel. *Phys. Fluids* **17** (8), 082102.
- FUJIOKA, H., HALPERN, D., RYANS, J. & GAVER III, D. P. 2016 Reduced-dimension model of liquid plug propagation in tubes. *Phys. Rev. Fluids* **1** (5), 053201.
- FUJIOKA, H., TAKAYAMA, S. & GROTBORG, J. B. 2008 Unsteady propagation of a liquid plug in a liquid-lined straight tube. *Phys. Fluids* **20** (6), 062104.
- GRIESE, M., BIRRER, P. & DEMIRSOY, A. 1997 Pulmonary surfactant in cystic fibrosis. *Eur. Respir. J.* **10** (9), 1983–1988.
- GROTBORG, J. B. 2011 Respiratory fluid mechanics. *Phys. Fluids* **23** (2), 021301.
- GUNTHER, A., KHAN, S. A., THALMANN, M., TRACHSEL, F. & JENSEN, K. F. 2004 Transport and reaction in microscale segmented gas-liquid flow. *Lab Chip* **4** (4), 278–286.
- GUTTFINGER, C. & TALLMADGE, J. A. 1965 Films of non-newtonian fluids adhering to flat plates. *AIChE* **11** (3), 403–413.
- HAVRE, K., STORNES, K. O. & STRAY, H. 2000 Taming slug flow in pipelines. *ABB review* **4**, 55–63.
- HAZEL, A. L. & HEIL, M. 2002 The steady propagation of a semi-infinite bubble into a tube of elliptical or rectangular cross-section. *J. Fluid Mech.* **470**, 91–114.
- HEIL, M., HAZEL, A. L. & SMITH, J. A. 2008 The mechanics of airway closure. *Resp. Physiol. Neurobi.* **163** (1), 214–221.
- HEWSON, R. W., KAPUR, N. & GASKELL, P. 2009 A model for film-forming with newtonian and shear-thinning fluids. *J. Fluid Mech.* **162**, 21–28.
- HIRASAKI, G. J., LAWSON, J. B. & OTHERS 1985 Mechanisms of foam flow in porous media: apparent viscosity in smooth capillaries. *Soc. Petrol Eng. J.* **25** (02), 176–190.
- HOFFMAN, R. L. 1975 A study of the advancing interface. i. interface shape in liquid-gas systems. *J. Colloid Interf. Sci.* **50** (2), 228–241.
- HOHLFELD, J. M. 2001 The role of surfactant in asthma. *Resp. Res.* **3** (1), 1.
- HOWELL, P. D., WATERS, S. L. & GROTBORG, J. B. 2000 The propagation of a liquid bolus along a liquid-lined flexible tube. *J. Fluid Mech.* **406**, 309–335.
- HU, Y., BIAN, S., GROTBORG, J., FILOCHE, M., WHITE, J., TAKAYAMA, S. & GROTBORG, J. B. 2015 A microfluidic model to study fluid dynamics of mucus plug rupture in small lung airways. *Biomicrofluidics* **9** (4), 044119.
- HUGHES, J. M., ROSENZWEIG, D. Y. & KIVITZ, P. B. 1970 Site of airway closure in excised dog lungs: histologic demonstration. *J. Appl. Physiol.* **29** (3), 340–344.
- HUH, D., FUJIOKA, H., TUNG, Y., FUTAI, N., PAINE, R., GROTBORG, J. B. & TAKAYAMA, S. 2007 Acoustically detectable cellular-level lung injury induced by fluid mechanical stresses in microfluidic airway systems. *Proc. Natl. Acad. Sci. U. S. A.* **104** (48), 18886–18891.
- JALAAI, M. & BALMFORTH, N. J. 2016 Long bubbles in tubes filled with viscoplastic fluid. *J. Non-Newtonian Fluid Mech.* **238**, 100–106.
- KAMM, R. D. & SCHROTER, R. C. 1989 Is airway closure caused by a liquid film instability? *Respir. Physiol.* **75** (2), 141–156.
- KLASEBOER, E., GUPTA, R. & MANICA, R. 2014 An extended bretherton model for long taylor bubbles at moderate capillary numbers. *Phys. Fluids* **26** (3), 032107.
- KREUTZER, M. T., KAPTEIJN, F., MOULIJN, J. A., KLEIJN, C. R. & HEISZWOLF, J. J. 2005 Inertial and interfacial effects on pressure drop of taylor flow in capillaries. *AIChE J.* **51** (9), 2428–2440.
- LABORIE, B., ROUYER, F., ANGELESCU, D. E. & LORENCEAU, E. 2017 Yield-stress fluid deposition in circular channels. *J. Fluid Mech.* **818**, 838–851.
- LADOSZ, A., RIGGER, E. & VON ROHR, P. R. 2016 Pressure drop of three-phase liquid-liquid-gas slug flow in round microchannels. *Microfluid. Nanofluid.* **20** (3), 1–14.
- LENORMAND, R., ZARCONI, C. & SARR, A. 1983 Mechanisms of the displacement of one fluid by another in a network of capillary ducts. *J. Fluid Mech.* **135**, 337–353.
- MAGNIEZ, J. C., BAUDOIN, M., LIU, C. & ZOUESHTIAGH, F. 2016 Dynamics of liquid plugs in prewetted capillary tubes: from acceleration and rupture to deceleration and airway obstruction. *Soft Matter* **12** (42), 8710–8717.
- NIMMO, A. J., CARSTAIRS, J. R., PATOLE, S. K., WHITEHALL, J., DAVIDSON, K. & VINK, R.

- 2002 Intratracheal administration of glucocorticoids using surfactant as a vehicle. *Clin. Exp. Pharmacol. P.* **29** (8), 661–665.
- PARK, C. W. & HOMSY, G. M. 1984 Two-phase displacement in hele shaw cells: theory. *J. Fluid Mech.* **139**, 291–308.
- RATULOWSKI, JOHN & CHANG, HSUEH-CHIA 1989 Transport of gas bubbles in capillaries. *Phys. Fluids A-Fluid* **1** (10), 1642–1655.
- SONG, Y., BAUDOIN, M., MANNEVILLE, P. & BAROUD, C. N. 2011 The air-liquid flow in a microfluidic airway tree. *Med. Eng. Phys.* **33** (7), 849–856.
- STARK, J. & MANGA, M. 2000 The motion of long bubbles in a network of tubes. *Transport Porous Med.* **40** (2), 201–218.
- SURESH, V. & GROTBORG, J. B. 2005 The effect of gravity on liquid plug propagation in a two-dimensional channel. *Phys. Fluids* **17** (3), 031507.
- TANNER, L. H. 1979 The spreading of silicone oil drops on horizontal surfaces. *J. Phys. D Appl. Phys.* **12** (9), 1473.
- TAYLOR 1961 Deposition of a viscous fluid on the wall of a tube. *J. Fluid Mech.* **10** (02), 161–165.
- VAN'T VEEN, A., WOLLMER, P., NILSSON, L. E., GOMMERS, D., MOUTON, J. W., KOOLJ, P. P. M. & LACHMANN, B. 1998 Lung distribution of intratracheally instilled tc-99m-tobramycin-surfactant mixture in rats with a klebsiella pneumoniae lung infection. *ACP- Appl. Cardiopul. P.* **7** (2), 87–94.
- VAUGHAN, B. L. & GROTBORG, J. B. 2016 Splitting of a two-dimensional liquid plug at an airway bifurcation. *J. Fluid Mech.* **793**, 1–20.
- WARNIER, M. J. F., DE CROON, M. H. J. M., REBROV, E. V. & SCHOUTEN, J. C. 2010 Pressure drop of gas-liquid taylor flow in round micro-capillaries for low to intermediate reynolds numbers. *Microfluid. Nanofluid.* **8** (1), 33–45.
- WATERS, S. L. & GROTBORG, J. B. 2002 The propagation of a surfactant laden liquid plug in a capillary tube. *Phys. Fluids* **14** (2), 471–480.
- WEISS, E. B., FALING, L. J., MINTZ, S., BROOKS, S. M., CHODOSH, S. & SEGAL, M. S. 1969 Acute respiratory failure in chronic obstructive pulmonary disease: Part i: Pathology. *Dm-Dis. Mon.* **15** (11), 1–58.
- WHITE, J. P. & HEIL, M. 2005 Three-dimensional instabilities of liquid-lined elastic tubes: A thin-film fluid-structure interaction model. *Phys. Fluids* **17** (3), 031506.
- WONG, H., RADKE, C. J. & MORRIS, S. 1995a The motion of long bubbles in polygonal capillaries. part 1. thin films. *J. Fluid Mech.* **292**, 71–94.
- WONG, H., RADKE, C. J. & MORRIS, S. 1995b The motion of long bubbles in polygonal capillaries. part 2. drag, fluid pressure and fluid flow. *J. Fluid Mech.* **292**, 95–110.
- WRIGHT, S. M., HOCKEY, P. M., ENHORNING, G., STRONG, P., REID, K. B. M., HOLGATE, S. T., DJUKANOVIC, R. & POSTLE, A. D. 2000 Altered airway surfactant phospholipid composition and reduced lung function in asthma. *J. Appl. Physiol.* **89** (4), 1283–1292.
- ZAMANKHAN, P., HELENBROOK, B. T., TAKAYAMA, S. & GROTBORG, J. B. 2012 Steady motion of bingham liquid plugs in two-dimensional channels. *J. Fluid Mech.* **705**, 258–279.
- ZHENG, Y., FUJIOKA, H., BIAN, S., TORISAWA, Y., HUH, D., TAKAYAMA, S. & GROTBORG, J. B. 2009 Liquid plug propagation in flexible microchannels: a small airway model. *Phys. Fluids* **21** (7), 071903.
- ZHENG, Y., FUJIOKA, H. & GROTBORG, J. B. 2007 Effects of gravity, inertia, and surfactant on steady plug propagation in a two-dimensional channel. *Phys. Fluids* **19** (8), 082107.